AIP | Review of Scientific Instruments

Real-time radiative divertor feedback control development for the NSTX-U tokamak using a vacuum ultraviolet spectrometer

V. A. Soukhanovskii, R. Kaita, and B. Stratton

Citation: Review of Scientific Instruments **87**, 11D605 (2016); doi: 10.1063/1.4960058
View online: http://dx.doi.org/10.1063/1.4960058
View Table of Contents: http://scitation.aip.org/content/aip/journal/rsi/87/11?ver=pdfcov
Published by the AIP Publishing

Real-time radiative divertor feedback control development for the NSTX-U tokamak using a vacuum ultraviolet spectrometer

V. A. Soukhanovskii,[1,a)] R. Kaita,[2] and B. Stratton[2]
[1]*Lawrence Livermore National Laboratory, 7000 East Ave., Livermore, California 94550, USA*
[2]*Princeton Plasma Physics Laboratory, 100 Stellarator Rd., Princeton, New Jersey 08543, USA*

(Presented 6 June 2016; received 6 June 2016; accepted 6 July 2016;
published online 4 August 2016)

A radiative divertor technique is planned for the NSTX-U tokamak to prevent excessive erosion and thermal damage of divertor plasma-facing components in H-mode plasma discharges with auxiliary heating up to 12 MW. In the radiative (partially detached) divertor, extrinsically seeded deuterium or impurity gases are used to increase plasma volumetric power and momentum losses. A real-time feedback control of the gas seeding rate is planned for discharges of up to 5 s duration. The outer divertor leg plasma electron temperature T_e estimated spectroscopically in real time will be used as a control parameter. A vacuum ultraviolet spectrometer McPherson Model 251 with a fast charged-coupled device detector is developed for temperature monitoring between 5 and 30 eV, based on the $\Delta n = 0, 1$ line intensity ratios of carbon, nitrogen, or neon ion lines in the spectral range 300–1600 Å. A collisional-radiative model-based line intensity ratio will be used for relative calibration. A real-time T_e-dependent signal within a characteristic divertor detachment equilibration time of ~10–15 ms is expected. *Published by AIP Publishing.* [http://dx.doi.org/10.1063/1.4960058]

I. INTRODUCTION

In order to mitigate high divertor heat loads and material erosion of divertor plasma-facing components (PFCs), a radiative (detached) divertor technique is used in nuclear fusion plasma device (tokamak) experiments.[1] The radiative divertor uses extrinsically seeded deuterium or impurity gases to increase volumetric power and momentum losses, and as a result to reduce heat and particle flux densities, both peak and average, on divertor target plates. The gas seeding has been shown to achieve the desired mitigation simultaneously with acceptable pedestal and core confinement in several tokamak experiments via a real-time feedback control of the gas injection rate.[2–7]

In the National Spherical Torus Experiment Upgrade (NSTX-U),[8] a medium-size spherical tokamak with graphite and eventually molybdenum PFCs and high projected divertor heat flux ($q_{peak} \leq 15$ MW/m^2, $q_{\parallel} \leq 200$ MW/m^2),[9] radiative divertor experiments are planned. Based on the NSTX experiments,[10–13] magnetic divertor geometry (i.e., the snowflake configuration[14]) and the radiative divertor technique[13] applied to the lower and upper divertors are the leading divertor heat flux mitigation strategies. A conceptual implementation of the real-time radiative divertor control system on NSTX-U has been previously described.[15] The system includes (1) a gas injection system (actuator) with two toroidally separated divertor outlets and a characteristic time response of ~50 ms; (2) a divertor cryo-condensation pump for gas removal; (3) a plasma control system module with multiple input, multiple output capabilities; and (4) control sensors. Several NSTX diagnostic measurements have been considered as control sensor candidates.[15] However, to make the radiative divertor control independent of specific discharge parameters (e.g., input power, plasma current, density, plasma radiation, and neutral pressure), we consider divertor plasma electron temperature T_e as a control parameter.

For real-time feedback control purposes, divertor T_e can be estimated with reduced accuracy or on a relative scale using Langmuir probes, thermoelectric current measurements,[7] or spectroscopically. A vacuum ultraviolet (VUV) spectrometer-based diagnostic has been developed for T_e monitoring in the range $5 \leq T_e \leq 30$ eV, based on $\Delta n = 0, 1$ emission line intensity ratios of carbon, nitrogen, or neon ions in the spectral range 300-1600 Å. A collisional-radiative model-based line intensity ratio is used for relative calibration. The design and laboratory testing of the diagnostic with a fast fiber-optically coupled detector system is described. During radiative detachment, strong deuterium high-n (Balmer, Paschen, and Brackett) series line emissions are observed in the strike point region due to volumetric recombination.[16,17] We plan to use them for estimates of $T_e \leq 2$ eV with another, ultraviolet, spectrometer system to be described elsewhere.

II. METHOD

During radiative divertor detachment, a parallel T_e gradient is developed in the divertor leg below the X-point. When low-Z impurities carbon or nitrogen are used to induce significant radiative losses, a radiation front is formed at 7-15 eV. Due to T_e-dependence of both the ionization-recombination balance and the electron impact excitation rates of resonant lines, the berillium-like and lithium-like ions become main radiators. A major fraction of divertor power loss occurs via $\Delta n = 0, 1, 2$ transitions of these ions corresponding

Note: Contributed paper, published as part of the Proceedings of the 21st Topical Conference on High-Temperature Plasma Diagnostics, Madison, Wisconsin, USA, June 2016.
a)Electronic mail: vlad@llnl.gov

TABLE I. Selected unblended carbon and nitrogen ion $\Delta n = 0$ and $\Delta n = 1$ emission lines that can form T_e-sensitive line intensity ratios.

		Wavelength (Å)	
Isosequence	Transition	Carbon	Nitrogen
Li I	$2s\ ^2S_{1/2}-2p\ ^2P_{3/2}$	1548.2	1238.8
	$2s\ ^2S_{1/2}-2p\ ^2P_{1/2}$	1550.8	1242.8
	$2p\ ^2P-3s\ ^2S$	419.6	266.3
	$2s\ ^2S-3p\ ^2P$	312.4	209.3
Be I	$2s^2\ ^1S_0-2s2p\ ^1P_1$	977.0	765.2
	$2s2p\ ^3P-2p^2\ ^3P$	1175.6	923.1
	$2s2p\ ^3P-2s3s\ ^3S$	538.2	322.6
	$2s2p\ ^3P-2s3d\ ^3D$	459.6	335.0

to vacuum ultraviolet lines in the range 150–1600 Å. The line intensity ratios of the $\Delta n = 0$ lines and $\Delta n = 1, 2, 3, \ldots$ lines are T_e-sensitive due to different excitation rate sensitivities. Table I shows the lines that were selected as candidates for T_e estimates. These bright VUV lines have been observed in tokamak divertors.[7,18–20] The line list is limited to $\Delta n = 0, 1$ transitions even though $\Delta n = 2, 3$ transitions may be observed in the divertor. Shown in Fig. 1 are the C III and C IV line intensity ratios. Similar T_e-sensitive line ratios are obtained for nitrogen or neon. Photon emission coefficients (PECs) from the ADAS database[21] were used; however, other collisional-radiative calculations based on different atomic rates give similar results.[20] The intensity ratios vary by a factor of 10 or more in the range 5-30 eV, suggesting the possibility of a reliable relative T_e-sensitive signal characteristic of the prevailing divertor leg T_e in the line-of-sight region. The intensity ratios of the C IV $\Delta n = 1; 2$ lines have been recently used for tokamak divertor T_e estimates in the range 20-60 eV with an accuracy of 20%.[22]

III. RESULTS AND DISCUSSION

A. VUV spectrometer

The spectrometer is mounted on an NSTX-U vacuum vessel horizontal divertor port with a direct local view of the divertor plasma. Shown in Fig. 2 are the placement and layout of the VUV system. The line of sight enables local

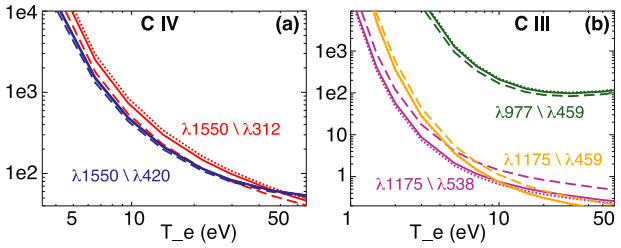

FIG. 1. Electron temperature sensitive line intensity ratios of $\Delta n = 0$ to $\Delta n = 1$ transitions of carbon ions. (a) C IV lines represent three typical divertor densities as follows: 4.92×10^{-19} m^{-3} (·····); 1.64×10^{-20} m^{-3} (——); and 4.92×10^{-20} m^{-3} (- - -). (b) C III lines represent three typical divertor densities as follows: 5×10^{-19} m^{-3} (·····); 1×10^{-20} m^{-3} (——); and 5×10^{-20} m^{-3} (- - -).

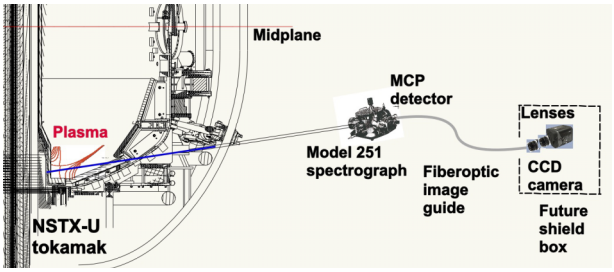

FIG. 2. Spectrometer placement on NSTX-U with a local line-of-sight of the divertor region.

measurements in the outer divertor leg, with measured line-integrated brightnesses weighted by the radiation front plasma parameters. The main elements of the spectrometer system include a spectrograph, a VUV image intensifier, an optical signal relay, and a charge-coupled device (CCD) detector. The spectrometer consists of the commercial McPherson Model 251 spectrograph[23] also known as Survey, Poor Resolution, Extended Domain (SPRED) spectrometer[24] and a micro-channel plate (MCP) VUV image intensifier. The Model 251 is a 292.1 mm flat-field spectrograph with aberration corrected toroidal gratings mounted at 71° angle of incidence. A turret with two gratings, 290 groove/mm and 2405 groove/mm, is mounted inside a spectrograph vacuum housing. An entrance slit is equipped with two micrometer feedthroughs that enable slit widths in the range 5-2000 μm and slit heights up to 10 mm.

The 290 (2405) groove/mm grating provides 1.6 (0.5) Å resolution and the spectral range 155-1700 Å (95-320 Å) in the focal plane. An 40 mm MCP image intensifier is mounted in the focal plane on a translator that allows fine adjustments of the spectral range. The dispersed VUV emission is incident on the CsI photocathode producing electrons that are accelerated in micro-channels with an applied potential of up to 1 kV. The electrons are further accelerated and proximity-focused by an additional potential of up to 5 kV applied to the P46 ($Y_3Al_5O_{12}$:Ce) phosphor scintillator. The P46 emission spectrum peaks at 5500 Å (green), and its time response is ≤100 ns. The phosphor is deposited on a fiberoptic taper that demagnifies the MCP image from 40 to 25 mm. Hence, the image intensifier provides a 25-mm diameter fiberoptic faceplate on the air side of the detector vacuum housing.

In the past, SPRED systems used a photodiode array coupled directly to the fiberoptic faceplate. However, the detector port makes it difficult to design a shield box around the detector assembly. Effective shielding from electromagnetic noise, energetic neutrons, gamma, and X-rays is necessary in the tokamak environment. We have developed a new optical coupling scheme between an optical detector and the MCP faceplate. The imaging optics provides a nearly 1:1 optical relay from the MCP faceplate to the CCD camera. A custom-built Schott coherent fiberoptic glass bundle (flexible image guide) is coupled directly to the MCP faceplate. The fiberoptic bundle is 3.8 m long and has a cross section of 4×25 mm. The bundle is constructed from sub-bundles each 60×60 μm, which are in turn constructed from individual 10 μm fibers. The output of the bundle is optically imaged on the CCD

camera using two Nikon $f = 50$ mm $f/1.8$ F-mount lenses that form an infinity conjugated lens pair. The CCD camera is a Princeton Instruments ProEM camera with the CCD chip size 25.6×3.2 mm. The CCD chip format is 1600×200 pixels, each pixel is a square with a 16 μm side. The CCD provides high quantum efficiency with the full well capacity of 350 ke^- and a linear gain from 1 to 1000 using electron multiplication technology. When the CCD is operated in a fully binned mode, read-out times as low as 0.7 ms can be achieved. A single row can be read-out in 0.22 ms.

B. Application for radiative divertor control

The 290 groove/mm grating in combination with the described detection system provides an extended spectral coverage that enables measurements of all $\Delta n = 1, 2, 3, \ldots$ lines of interest simultaneously. The wavelength calibration will be accomplished using the tokamak spectra, as was done in similar instruments.[18,19,22,25] A preliminary wavelength calibration is described below. A photometric (and a relative) calibration of the entire diagnostic can be accomplished using either a laboratory radiometric calibration standard, i.e., at a synchrotron facility,[26] or a branching ratio method using a photometrically calibrated visible spectrometer with the same line of sight.[25] The T_e estimates can be compared for consistency with surface Langmuir probe measurements, or with direct T_e measurements using a divertor Thomson scattering system. The latter system is presently planned for NSTX-U.[27] However, for radiative divertor control in the near-term, we plan to develop functional relations between the desired state of divertor detachment based on multiple divertor diagnostics (i.e., infrared thermography, Balmer line spectroscopy, Langmuir probes, and bolometry) and the relative T_e line ratio signal from the VUV spectrometer.

C. Laboratory detector characterization

Before mounting the spectrometer on NSTX-U, system performance was characterized in the laboratory. A Hamamatsu L10366 high-brightness deuterium lamp was used as an emission source. The lamp is enclosed in a vacuum housing, however, to maintain ultra-high vacuum in the spectrometer housing to avoid MCP arcing at vacuum 2×10^{-6} Torr or higher, it was necessary to isolate the lamp with a MgF_2 window. The window VUV transmission cutoff is at about 1150 Å. The lamp provided a point source of intense VUV emission. An example of the VUV spectrum recorded by the spectrometer system is shown in Fig. 3. The spectrum consists of a sharp deuterium Lyman-α atomic transition $2p - 1s$ at 1215.7 Å, and a molecular D_2 spectrum that includes rotational-vibrational $C\,^1\Pi_u - X\,_1\Sigma_g^+$ Werner and $B_1\Sigma_u^+ - X\,_1\Sigma_g^+$ Lyman bands.[28] The longest wavelength feature of the D_2 Lyman band spectrum is at 1610 Å. It was used to adjust the MCP in the focal plane to enable C IV λ1550 line measurements. The preliminary wavelength calibration performed using the identified D_2 Werner and Lyman band peaks confirms the expected spectral coverage for low-Z impurity lines. It also shows that further optimization, i.e., magnification by 10%-20%, is possible in order to improve spectral resolution.

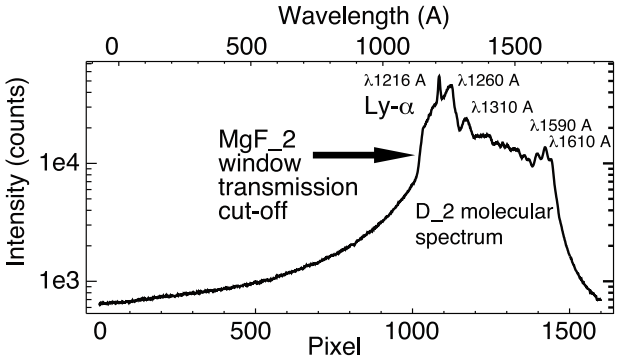

FIG. 3. Deuterium lamp VUV spectrum measured through a MgF_2 window by SPRED with a 290 l/mm grating.

The MCP image intensifier can be operated in a range of MCP and phosphor voltages enabling gain and proximity focusing adjustments over a large range. Shown in Fig. 4 are the MCP and phosphor voltage scans elucidating the typical gain ranges. The spectral feature at λ1260 Å integrated over a band of 10 Å was used. The MCP gain could be varied by over two orders of magnitude. Varying the phosphor potential resulted in intensity variations within a factor of 10. The desirable mode of MCP operation is to utilize the minimal voltages that provide adequate MCP gain and best spatial resolution, determined by charge spreading at high V_{ph}. The MCP detector is also susceptible to increased micro-arcing at high V_{MCP} and V_{ph}.

D. Resolution of the optical relay and detector

An introduction of the optical relay resulted in some degradation of spectral resolution. The nominal spectrometer resolution is defined in terms of the Rayleigh criterion applied to two spectral line images on the MCP faceplate. The spectral resolution is mainly determined by the spectrometer linear dispersion and the detector spatial resolution. It is 0.5 Å for the 2405 groove/mm grating and 1.6 Å for the 290 groove/mm grating.[23] To minimize the spectral resolution degradation, the optical relay and detector system should provide spatial resolution of 40 μm or better, to match the spatial resolution on the MCP image intensifier. Laboratory imaging tests were conducted to characterize the spatial resolution of the entire optical relay and detection system. The NBS 1963A resolution target from Thorlabs was attached directly to the fiberoptic

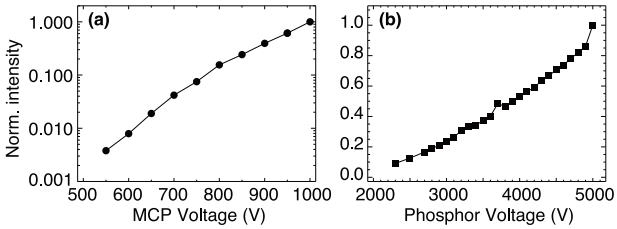

FIG. 4. Normalized detector sensitivity as a function of voltage (a) on MCP, at fixed $V_{ph} = 4500$ V; (b) on phosphor, at fixed $V_{MCP} = 950$ V.

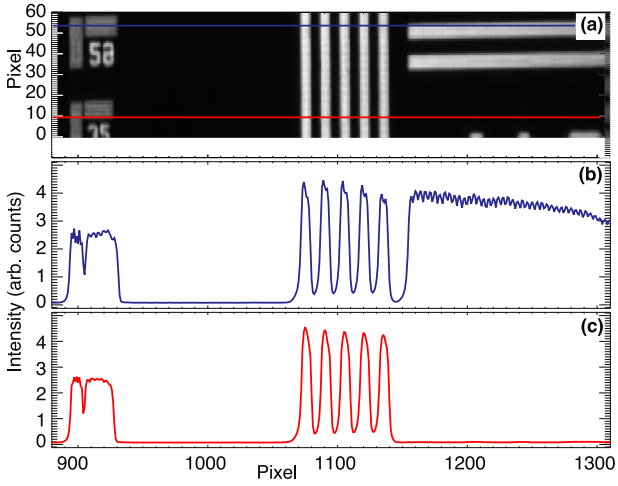

FIG. 5. A combined optical resolution of the optical detection system. (a) A partial image of the 1963A NBS optical resolution target showing line sets of 29, 35, and 10 line pairs / mm; (b) intensity distribution of pixel row 55; (c) same of pixel row 10.

bundle simulating the MCP faceplate. Shown in Fig. 5 are the image and intensity distributions recorded in this test. Seen on the image are the sets comprising 10, 29, and 32 cycles/mm, corresponding to spatial resolutions of 100, 34, and 31 μm, respectively. The last line pair set is barely resolved, suggesting the lower spatial resolution limit of the combined optical relay, coupling lenses, and the CCD detector to be on the order of 30 μm, or 2-3 pixels of the relay and detector components. Hence, it is consistent with the fiber size of 10 μm, the lens resolution of ~20 μm (estimated as the Airy disk size of $\sim 1.22\lambda f/d$, where λ is the light wavelength, and d is the lens diameter), and the CCD pixel size of 16 μm. The image also shows an undesirable fiberoptic sub-bundle edge effect resulting in 10% intensity modulation from a uniform light field. Filtering out these periodic intensity modulations via Fourier-transform based software filters is considered.

In conclusion, a new VUV spectrometer system has been developed for NSTX-U divertor research. The primary goal of this system is to validate T_e-sensitive line intensity ratio measurements of C III and C IV carbon ions for real-time radiative divertor feedback control. The overall time response of the system is several ms, lower than the actuator (gas system) response time (~50 ms) and the characteristic detachment onset time (≤10 ms). Other applications of this system with the 290 groove/mm grating include studies of molecular D_2 spectral Werner and Lyman bands and spectroscopy of lower ionization charge states of molybdenum (when molybdenum PFCs are installed in NSTX-U divertor). With the 2405 groove/mm grating, studies of Li III Lyman series emissions are planned in support of the lithium divertor vapor shielding experiments.

The digital data for this paper can be found in http://arks.princeton.edu/ark:/88435/dsp014x51hm47x.

ACKNOWLEDGMENTS

The authors would like to thank A. Brereton and R. Ellis for engineering support, G. Smalley and T. Holoman for technical support, and G. Zimmer for computer support. This work was supported by the US Department of Energy under Contract Nos. DE-AC52-07NA27344 and DE-AC02-09CH11466.

[1]A. Loarte *et al.*, Nucl. Fusion **47**, S203 (2007).
[2]G. L. Jackson *et al.*, J. Nucl. Mater. **241-243**, 618 (1997).
[3]J. Bucalossi *et al.*, J. Nucl. Mater. **290-293**, 566 (2001).
[4]H. Tamai *et al.*, Fusion Eng. Des. **39-40**, 163 (1998).
[5]H. Tamai *et al.*, J. Nucl. Mater. **266-269**, 1219 (1999).
[6]B. Lipschultz *et al.*, J. Nucl. Mater. **241-243**, 771 (1997).
[7]A. Kallenbach *et al.*, Plasma Phys. Controlled Fusion **52**, 055002 (2010).
[8]J. E. Menard *et al.*, Nucl. Fusion **52**, 083015 (2012).
[9]T. K. Gray *et al.*, J. Nucl. Mater. **415**, S360 (2011).
[10]V. A. Soukhanovskii *et al.*, J. Nucl. Mater. **337-339**, 475 (2005).
[11]V. A. Soukhanovskii *et al.*, J. Nucl. Mater. **363-365**, 432 (2007).
[12]V. A. Soukhanovskii *et al.*, Phys. Plasmas **16**, 022501 (2009).
[13]V. A. Soukhanovskii *et al.*, Nucl. Fusion **49**, 095025 (2009).
[14]V. A. Soukhanovskii *et al.*, Nucl. Fusion **51**, 012001 (2011).
[15]V. A. Soukhanovskii *et al.*, Rev. Sci. Instrum. **83**, 10D716 (2012).
[16]V. A. Soukhanovskii *et al.*, Rev. Sci. Instrum. **77**, 10127 (2006).
[17]V. A. Soukhanovskii, A. G. McLean, and S. L. Allen, Rev. Sci. Instrum. **85**, 11E418 (2014).
[18]M. E. Fenstermacher *et al.*, J. Nucl. Mater. **241-243**, 666 (1997).
[19]C. F. Maggi *et al.*, J. Nucl. Mater. **241-243**, 414 (1997).
[20]V. A. Soukhanovskii *et al.*, Rev. Sci. Instrum. **70**, 340 (1999).
[21]H. P. Summers, The ADAS User Manual, version 2.6, www.adas.ac.uk, 2004.
[22]K. D. Lawson *et al.*, Plasma Phys. Controlled Fusion **53**, 015002 (2011).
[23]McPherson Inc., http://www.mcphersoninc.com, 2016.
[24]R. Fonck, A. Ramsey, and R. Yelle, Appl. Opt. **21**, 2115 (1982).
[25]K. D. Lawson *et al.*, J. Instrum. **4**, P04013 (2009).
[26]B. C. Stratton *et al.*, Rev. Sci. Instrum. **57**, 2043 (1986).
[27]A. G. McLean *et al.*, Rev. Sci. Instrum. **85**, 11E825 (2014).
[28]J. M. Ajello, S. K. Srivastava, and Y. L. Yung, Phys. Rev. A **25**, 2485 (1982).